

# BER Analysis and Optimization of Pinching-Antenna-Based NOMA Communications

Mahmoud AlaaEldin, Amy S. Inwood, Xidong Mu, and Michail Matthaiou  
Centre for Wireless Innovation (CWI), Queen's University Belfast, Belfast BT3 9DT, U.K.  
Emails: {m.alaieldin, a.inwood, x.mu, m.matthaiou}@qub.ac.uk

**Abstract**—This paper presents the first bit error rate (BER) analysis of a pinching-antenna (PA)-based non-orthogonal multiple access (NOMA) communication system. The PA is assumed to be able to be placed anywhere along the waveguide and serves two NOMA user equipment (UEs) in both uplink (UL) and downlink (DL) scenarios. Exact closed-form expressions for the average BER of each user are derived under practical imperfect successive interference cancellation (SIC). These expressions are then used to optimize the PA location for minimizing the overall average BER of both UEs. In the UL case, the interference between the users' channels introduces phase-dependent fluctuations in the BER cost function, making it highly non-convex with many local extrema. To address this challenge, a smoothing technique is applied to extract the lower envelope of the BER function, effectively suppressing ripples and enabling a reliable identification of the global minimum. In the DL case, a joint optimization of the PA location and NOMA power allocation coefficients is proposed to minimize the average BER. Simulation results verify the accuracy of the analytical derivations and the effectiveness of the proposed optimization methods. Notably, the UL results demonstrate that an optimally positioned PA can create the required received power difference between two equally powered UEs for reliable power-domain NOMA decoding under imperfect SIC.

## I. INTRODUCTION

As applications, such as artificial intelligence, high-definition streaming, and augmented reality become commonplace, the demand for mobile connectivity is growing rapidly. Consequently, the demand for higher capacity and more efficient networks continues to intensify. One way to increase capacity is to increase the carrier frequency. However, this introduces greater propagation challenges, including stronger attenuation, stronger path loss, and higher sensitivity to blockages [1], making reliable access to line-of-sight (LoS) paths critical.

Pinching antenna systems (PASSs) are a recently proposed class of flexible antenna technologies, in which a dielectric particle, referred to as a pinching antenna (PA), is placed on a dielectric waveguide to radiate wireless signals [2], [3]. Spanning lengths in the order of meters, the dielectric waveguide provides the flexibility to reposition the PA over a large range, creating a LoS transceiver link. Note that PASSs differ from other flexible-antenna technologies, such as fluid antennas and movable antennas, where adjustments are limited

This work was supported by the U.K. Engineering and Physical Sciences Research Council (EPSRC) grant (EP/X04047X/2) for TITAN Telecoms Hub. The work of M. Matthaiou was supported by the European Research Council (ERC) under the European Union's Horizon 2020 research and innovation programme (grant agreement No. 101001331).

to the wavelength scale [3]. While PASSs enable reliable communications at high carrier frequencies, spectrum resources remain limited and must be used efficiently. Each waveguide in a PASS conveys an identical signal. Therefore, using power-domain (PD)-non-orthogonal multiple access (NOMA) with successive interference cancellation (SIC), which allows all user equipment (UEs) to simultaneously share the same resource block, in conjunction with PASSs can offer improved spectral efficiency.

Existing studies on the synergy between PASSs and NOMA have primarily focused on analyzing and optimizing system-level metrics, such as the sum rate [4]–[6]. However, there has been limited work on symbol-level metrics, which provide crucial insights into system reliability.

Therefore, in this work, we provide the first study on the bit error rate (BER) of PA-assisted NOMA, as well as the first study on PA-assisted NOMA with imperfect SIC decoding. We consider a fundamental two-user single-antenna PASS, where the PA can be located at any point on the waveguide, and investigate both uplink (UL) and downlink (DL) scenarios. Exact BER expressions are derived for the two users in the UL PD-NOMA scenario employing quadrature phase-shift keying (QPSK) modulation and considering imperfect SIC decoding. We then optimize the PA position to minimize the derived average UL BER. Finally, we propose a method to jointly optimize the PA position and power allocation coefficients in the DL PD-NOMA scenario employing general  $M$ -quadrature amplitude modulation (QAM) modulation to minimize the average BER of the users under imperfect SIC.

*Notation:* The probability of event  $A$  is denoted  $\Pr(A)$ ;  $\Pr(A | B)$  represents the probability of event  $A$  conditioned on event  $B$ ;  $P_e(\cdot)$  denotes the probability of error;  $\Re(z)$  and  $\Im(z)$  denote the real and imaginary components of complex number  $z$ , respectively;  $\angle z$  is the angle of complex number  $z$ ;  $\mathcal{CN}(\mu, \sigma^2)$  represents a complex Gaussian distribution with mean  $\mu$  and variance  $\sigma^2$ ;  $Q(\cdot)$  is the Gaussian Q-function, and  $\text{sgn}(\cdot)$  is the signum function.

## II. SYSTEM MODEL

Consider the PASS shown in Fig. 1, where a single-antenna base station (BS) serves two single-antenna UEs via a single PA. The PA can be activated at any point  $x$  on the waveguide of length  $L$ . The UEs are distributed within a  $D_1 \times D_2$  m<sup>2</sup> region, the BS is located at  $(x, y) = (0, 0)$ , and the waveguide is aligned along the  $x$ -axis with a vertical offset of  $d$  m.

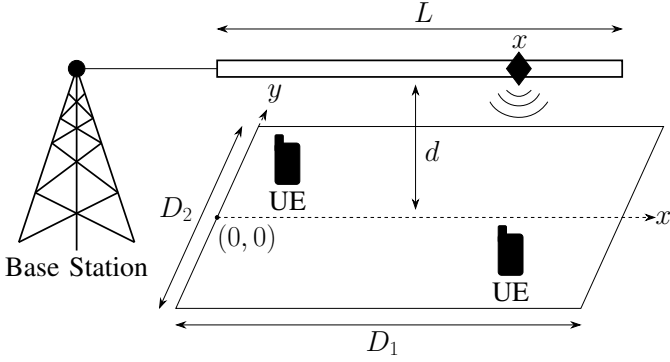


Fig. 1. A PA-based NOMA communication system with two users.

As the position of the PA can be chosen to guarantee LoS, and given that PAs are primarily intended for high-frequency deployments, the channels between the PA and the UEs are assumed to be purely LoS. Accordingly, the channel between UE  $k$  and the PA located at position  $x$  along the waveguide is modeled using the spherical-wave channel model [7], [8]:

$$h_k(x) = \frac{\eta e^{-j\frac{2\pi}{\lambda}|\psi_k - \psi_p(x)|}}{|\psi_k - \psi_p(x)|}, \quad (1)$$

where  $\psi_k = (x_k, y_k, 0)$  is the location of UE  $k$ ,  $\psi_p(x) = (x, 0, d)$  is the location of the PA as a function of  $x$ ,  $\eta = \frac{c}{4\pi f_c}$ ,  $c$  is the speed of light in a vacuum,  $f_c$  is the carrier frequency and  $\lambda$  is the wavelength. Additionally, we model the loss from the signal traveling within the waveguide as [3]

$$P_L(x) = 10^{-\frac{\kappa}{20}|\psi_p(0) - \psi_p(x)|} e^{-j\frac{2\pi}{\lambda_g}|\psi_p(0) - \psi_p(x)|}, \quad (2)$$

where  $\kappa$  is the average attenuation factor along the dielectric waveguide in dB/m,  $\lambda_g = \frac{\lambda}{n_{\text{eff}}}$  is the guided wavelength, and  $n_{\text{eff}}$  is the effective refractive index of the dielectric waveguide. Therefore, the channel between UE  $k$  and the BS via a PA located at  $x$  is

$$\tilde{h}_k(x) = P_L(x)h_k(x). \quad (3)$$

#### A. Uplink scenario

In the UL scenario, each UE transmits its own signal, both of which are received by the PA. Thus, the total superimposed received NOMA signal at the BS can be written as

$$y^{\text{UL}} = \sqrt{P_1}\tilde{h}_1(x)s_1 + \sqrt{P_2}\tilde{h}_2(x)s_2 + n, \quad (4)$$

where  $P_1$  and  $P_2$  are the transmit powers of UEs 1 and 2, respectively,  $s_1$  and  $s_2$  are the signals corresponding to UEs 1 and 2, respectively, while  $n \sim \mathcal{CN}(0, 2\sigma^2)$  is the additive white Gaussian noise (AWGN). In the UL scenario, we assume that both UEs employ gray-coded QPSK modulation, such that  $s_k$  is drawn from the constellation  $\mathcal{S} = \{1+j, 1-j, -1-j, -1+j\}$ , corresponding respectively to the bit pairs  $(b_{k,1}, b_{k,2}) = (0, 1), (0, 0), (1, 0), (1, 1)$ .

#### B. Downlink scenario

In the DL scenario, the signals intended for different UEs are transmitted via a single radio-frequency chain. Therefore, they must be superimposed at the BS using different power coefficients prior to transmission. Hence, the received NOMA signal at the  $k$ -th UE can be given as

$$y_k^{\text{DL}} = \tilde{h}_k(x)s + n_k, \quad \forall k \in \{1, 2\}, \quad (5)$$

where

$$s = \sqrt{P_T} \left( \sqrt{\frac{\alpha}{\nu_1}}s_1 + \sqrt{\frac{1-\alpha}{\nu_2}}s_2 \right), \quad (6)$$

is the superimposed signal transmitted by the BS,  $P_T$  is the transmit power of the PA, and  $\alpha$  is the power allocation coefficient. The modulation symbol  $s_k = s_{k,I} + js_{k,Q}$  is drawn from a square QAM alphabet, where the in-phase and quadrature components of  $s_k$  can take values from the set  $\{\pm 1, \pm 3, \dots, \pm\sqrt{M_k}-1\}$ , while  $M_k$  is the modulation order of UE  $k$ . The scaling factor  $\nu_k = \frac{2}{3}(M_k-1)$  is used to normalize the power of  $s_k$  to unity.

### III. UPLINK AND DOWNLINK BER ANALYSIS

In this section, we present exact BER expressions for each UE in both the UL and DL scenarios by detailing the imperfect SIC detection process.

#### A. Uplink scenario

1) *BER Analysis of UE 1:* Without loss of generality, it is assumed that the received signal from UE 1 has a higher amplitude than that from UE 2 and is therefore decoded first, with the signal from UE 2 treated as interference. To decode  $s_1$ , the BS multiplies the total received signal in (4) by  $e^{-j\angle\tilde{h}_1(x)}$  to remove the phase shift of the channel, leading to

$$y_1^{\text{UL}} = \sqrt{P_1}\tilde{h}_1(x)|s_1 + \sqrt{P_2}\tilde{h}_2(x)e^{-j\angle\tilde{h}_1(x)}s_2 + ne^{-j\angle\tilde{h}_1(x)},$$

which aligns  $|\tilde{h}_1(x)|s_1$  with the QPSK constellation. The rotated received signal from UE 2 is treated as additional noise. The detection rule of  $s_1$  can now be given as

$$\hat{s}_1 = \hat{s}_{1,I} + j\hat{s}_{1,Q} = \text{sgn}(\Re(y_1^{\text{UL}})) + j\text{sgn}(\Im(y_1^{\text{UL}})). \quad (7)$$

The unconditional BER of UE 1 can be expressed as the average of the conditional BERs over all possible pairs of transmitted QPSK symbols  $(s_1, s_2)$ , such that

$$\text{BER}_1^{\text{UL}} = \frac{1}{4} \sum_{s_1 \in \mathcal{S}} \frac{1}{4} \sum_{s_2 \in \mathcal{S}} \text{BER}_{1|s_1, s_2}^{\text{UL}}. \quad (8)$$

The conditional BER, given a transmitted symbol pair  $(s_1, s_2)$ , can be expressed as the average of the detection error probabilities of its two individual bits, such that

$$\text{BER}_{1|s_1, s_2}^{\text{UL}} = \frac{1}{2} (P_e(b_{1,1} | s_1, s_2) + P_e(b_{1,2} | s_1, s_2)), \quad (9)$$

where  $b_{1,1}$  and  $b_{1,2}$  are the bits transmitted by UE 1, which are represented by the in-phase and quadrature components of  $s_1$ ,  $s_{1,I}$  and  $s_{1,Q}$ , respectively. The error probability of  $b_{1,1}$

and  $b_{1,2}$  is the likelihood that the Gaussian noise drives the received signal beyond the decision threshold of zero as

$$P_e(b_{1,1}|s_1, s_2) = \Pr(s_{1,I} \Re(y_1^{\text{UL}}) < 0) = Q\left(\frac{\mu_{b_{1,1}}}{\sigma}\right), \quad (10)$$

$$P_e(b_{1,2}|s_1, s_2) = \Pr(s_{1,Q} \Im(y_1^{\text{UL}}) < 0) = Q\left(\frac{\mu_{b_{1,2}}}{\sigma}\right), \quad (11)$$

where

$$\mu_{b_{1,1}} = \sqrt{P_1} |\tilde{h}_1(x)| + \sqrt{P_2} s_{1,I} \Re(\tilde{h}_2(x) e^{-j\angle \tilde{h}_1(x) s_2}),$$

$$\mu_{b_{1,2}} = \sqrt{P_1} |\tilde{h}_1(x)| + \sqrt{P_2} s_{1,Q} \Im(\tilde{h}_2(x) e^{-j\angle \tilde{h}_1(x) s_2}).$$

2) *BER Analysis of UE 2*: To decode  $s_2$ , the detected signal of UE 1,  $\sqrt{P_1} \tilde{h}_1(x) \hat{s}_1$ , is first subtracted from the received signal in (4). The residual is then multiplied by  $e^{-j\angle \tilde{h}_2(x)}$ , which aligns the desired UE 2 component with the QPSK constellation, yielding

$$y_2^{\text{UL}} = \sqrt{P_2} |\tilde{h}_2(x)| s_2 + \sqrt{P_1} \tilde{h}_1(x) \times e^{-j\angle \tilde{h}_2(x)} (s_1 - \hat{s}_1) + n e^{-j\angle \tilde{h}_2(x)}.$$

Again, treating the non-desired signal as additional noise, the received signal from UE 2 can be decoded as

$$\hat{s}_2 = \text{sgn}(\Re(y_2^{\text{UL}})) + j \text{sgn}(\Im(y_2^{\text{UL}})). \quad (12)$$

To determine the unconditional BER of UE 2, all possible transmitted symbols  $s_1$  and  $s_2$ , as well as all possible detected symbols  $\hat{s}_1$  must be considered. For each transmitted pair  $(s_1, s_2)$ ,  $\hat{s}_1$  may take any QPSK value, with probability  $\Pr(\hat{s}_1 = c | s_1, s_2), \forall c \in \mathcal{S}$ . After decoding  $\hat{s}_1$ , the contribution of UE 1 is subtracted via SIC, leaving a residual interference of  $R = s_1 - \hat{s}_1$  that may affect the detection of  $s_2$ . The conditional BER for UE 2 given this outcome is  $\text{BER}_{2|s_2, R}^{\text{UL}}$ . By the law of total probability, the unconditional BER of UE 2 is obtained by summing the conditional BER over all values of  $R$ , weighted by  $\Pr(R = r | s_2)$ , and subsequently averaging over all possible realizations of  $s_2$ , yielding

$$\text{BER}_2^{\text{UL}} = \frac{1}{4} \sum_{s_2 \in \mathcal{S}} \sum_{r \in \mathcal{R}} \Pr(R = r | s_2) \text{BER}_{2|s_2, R}^{\text{UL}}. \quad (13)$$

The values that  $R$  can take are determined by the  $\hat{s}_1$  outcomes of the detection process of  $s_1$ . Each of the 4 possibilities of  $s_1$  being transmitted has 4 possible decoded symbols, giving 16 outcomes in total, some of which produce the same residual due to symmetry. The 9 possible distinct residual values are

$$R = r, \quad r \in \mathcal{R} = \{0, \pm 2, \pm 2j, \pm 2 \pm 2j\}, \quad (14)$$

where  $r = 0$  corresponds to correct detection,  $r = \pm 2$  or  $\pm 2j$  to a single-bit error, and  $r = \pm 2 \pm 2j$  to errors in both bits. These values are illustrated in Fig 2.

To calculate the probability of  $R = r$  given  $s_2$ , let us define

$$\Pr(R = r | s_1, s_2) = \Pr(\hat{s}_1 = c : s_1 - c = r | s_1, s_2), \quad (15)$$

where  $r \in \mathcal{R}$  and  $c \in \mathcal{S}$ . The probability of a given residual is the sum of the probabilities of all  $(s_1, \hat{s}_1)$  pairs that lead to that

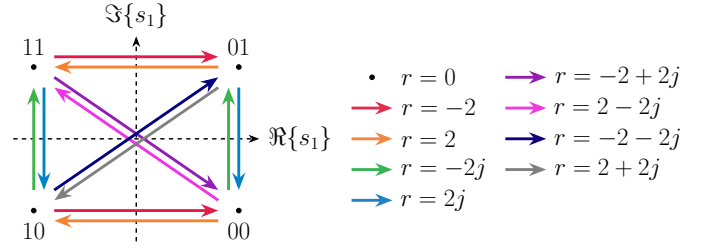


Fig. 2. Residual interference vectors  $r = s_1 - \hat{s}_1$ , drawn from the transmitted symbol  $s_1$  (origin) to the detected symbol  $\hat{s}_1$  (endpoint).

residual. As all  $s_1$  are equally likely, the explicit dependence on  $s_1$  can be removed by averaging over it, such that

$$\Pr(R = r | s_2) = \frac{1}{4} \sum_{s_1 \in \mathcal{S}} \Pr(R = r | s_1, s_2). \quad (16)$$

To evaluate  $\text{BER}_2^{\text{UL}}$ , expressions for  $\Pr(\hat{s}_1 = c | s_1, s_2)$  and  $\text{BER}_{2|s_2, R}^{\text{UL}}$  are required. As the Gaussian noise is circularly symmetric, and the in-phase and quadrature components are independent,  $\Pr(\hat{s}_1 = c | s_1, s_2)$  can be expressed as

$$\Pr(\hat{s}_1 = c | s_1, s_2) = \Pr(\hat{s}_{1,I} = c_I | s_1, s_2) \Pr(\hat{s}_{1,Q} = c_Q | s_1, s_2).$$

This reduces the two-dimensional QPSK decision rule to two independent one-dimensional detection problems along the in-phase and quadrature axes. The noise-free signal component along each axis can be defined as

$$\mu_{\hat{s}_{1,I}} = \sqrt{P_1} |\tilde{h}_1(x)| s_{1,I} + \sqrt{P_2} \Re(\tilde{h}_2(x) e^{-j\angle \tilde{h}_1(x) s_2}),$$

$$\mu_{\hat{s}_{1,Q}} = \sqrt{P_1} |\tilde{h}_1(x)| s_{1,Q} + \sqrt{P_2} \Im(\tilde{h}_2(x) e^{-j\angle \tilde{h}_1(x) s_2}).$$

Therefore, the detection probabilities along each axis are

$$\Pr(\hat{s}_{1,I} = c_I | s_1, s_2) = \Pr(-c_I \Re(y_2^{\text{UL}}) < 0) = Q\left(-c_I \frac{\mu_{\hat{s}_{1,I}}}{\sigma}\right), \quad (17)$$

$$\Pr(\hat{s}_{1,Q} = c_Q | s_1, s_2) = \Pr(-c_Q \Im(y_2^{\text{UL}}) < 0) = Q\left(-c_Q \frac{\mu_{\hat{s}_{1,Q}}}{\sigma}\right). \quad (18)$$

Note that the negative signs arise as (17) and (18) correspond to detection probabilities rather than error probabilities. Finally, following the same process as for  $\text{BER}_{1|s_1, s_2}^{\text{UL}}$ ,

$$\text{BER}_{2|s_2, R}^{\text{UL}} = \frac{1}{2} (P_e(b_{2,1} | s_2, R) + P_e(b_{2,2} | s_2, R)), \quad (19)$$

where  $b_{2,1}$  and  $b_{2,2}$  are the bits transmitted by UE 2, which are represented by the in-phase and quadrature components of  $s_2$ ,  $s_{2,I}$  and  $s_{2,Q}$ , respectively. The conditional error probability of  $b_{2,1}$  and  $b_{2,2}$  in (19) can be given as

$$P_e(b_{2,1} | s_2, R) = (s_{2,I} \Re(y_2^{\text{UL}}) < 0) = Q\left(\frac{\mu_{s_{2,1}}}{\sigma}\right), \quad (20)$$

$$P_e(b_{2,2} | s_2, R) = (s_{2,Q} \Im(y_2^{\text{UL}}) < 0) = Q\left(\frac{\mu_{s_{2,Q}}}{\sigma}\right), \quad (21)$$

and

$$\mu_{s_{2,1}} = \sqrt{P_2} |\tilde{h}_2(x)| + \sqrt{P_1} s_{2,I} \Re(\tilde{h}_1(x) e^{-j\angle \tilde{h}_2(x) R}),$$

$$\mu_{s_{2,Q}} = \sqrt{P_2} |\tilde{h}_2(x)| + \sqrt{P_1} s_{2,Q} \Im(\tilde{h}_1(x) e^{-j\angle \tilde{h}_2(x) R}).$$

## B. Downlink scenario

In the DL, each UE receives both transmitted signals multiplied by the same channel coefficient. Therefore, applying a phase shift of  $e^{-j\angle\tilde{h}_k(x)}$  at UE  $k$  to align  $\tilde{h}_k(x)s$  with the QAM constellation,

$$\tilde{y}_k^{\text{DL}} = |\tilde{h}_k(x)|s + n_k e^{-j\angle\tilde{h}_k(x)}. \quad (22)$$

The unconditional average BER of UE  $k$  was derived in [9] as

$$\text{BER}_k^{\text{DL}} = \sum_{q=1}^{N_Q} c_q Q \left( \frac{\sqrt{P_T} |\tilde{h}_k(x)| (a_{1,q} \sqrt{\frac{\alpha}{\nu_1}} + a_{2,q} \sqrt{\frac{1-\alpha}{\nu_2}})}{\sigma} \right), \quad (23)$$

where  $N_Q$  is the total number of  $Q(\cdot)$  functions in the conditional BER expression of UE  $k$ , and  $a_{1,q}$ ,  $a_{2,q}$  and  $c_q$  are constants that depend on the modulation order and can be calculated using [9, Algorithm 1].

## IV. BER MINIMIZATION-BASED OPTIMIZATION OF THE PA-BASED NOMA SYSTEM

In this section, we propose optimization schemes to minimize the average BER of the two UEs in the UL and DL.

### A. Optimization of the UL scenario

In the UL scenario, the location of the PA can be adjusted to create a sufficient difference in the received power from the 2 UEs at the BS and thus facilitate successful SIC-based PD-NOMA decoding. To achieve this, the PA can be positioned closer to the stronger UE (in this case, UE 1, without loss of generality), which is the first user in the SIC decoding order. This placement reduces the path loss associated with the stronger UE and ensures that its received signal at the BS has a higher power level than that of the weaker user (in this case, UE 2). This PA placement reduces the decoding error of  $s_1$  (where  $s_2$  acts as interference) and thereby mitigates the error propagation caused by imperfect SIC when subtracting  $\sqrt{P_1} \tilde{h}_1(x) \hat{s}_1$  from the received signal  $y^{\text{UL}}$  to decode  $s_2$ .

As the derived expressions of  $\text{BER}_1^{\text{UL}}$  and  $\text{BER}_2^{\text{UL}}$  are functions of the PA location,  $x$  can be optimized to minimize the average BER of the two users. Therefore, the optimization problem of  $x$  can be formulated as

$$\min_x f(x) = 10 \log_{10} (\text{BER}_1^{\text{UL}}(x) + \text{BER}_2^{\text{UL}}(x)), \quad (24a)$$

$$\text{s.t. } 0 \leq x \leq L, \quad (24b)$$

where the log transformation in (24a) is made to pronounce the structure of the objective function and ease the numerical search process. While the cost function has a clear trend, it rapidly fluctuates (as seen in Fig. 4 in Sec. V-A). These fluctuations are a result of the superposition of  $h_1(x)$  and  $h_2(x)$  at the PA. Each channel has a different phase shift, which causes constructive interference (local maxima) or destructive interference (local minima) with varying  $x$  as evident in (1).

Due to these fluctuations, directly optimizing  $f(x)$  with numerical methods, such as gradient descent, is impractical, as it quickly converges to local minima. Therefore, the moving

minimum sliding window technique is applied to produce a smooth version of  $f(x)$  for minimization. This technique computes the minimum value of  $f(x)$  within a local sliding window. For a discrete version of the function,  $f(nT)$ , where  $T$  denotes the sampling period, the operation is defined as

$$\bar{f}(x) = \min_{n \in W_x} f(nT), \quad (25)$$

where  $W_x$  denotes the set of indices within a window centered at  $x$ . This nonlinear filtering process is equivalent to a morphological erosion, effectively suppressing short-term peaks while preserving local minima. When applied to a non-smooth or noisy function, the resulting  $\bar{f}(x)$  provides a locally adaptive estimate of the lower envelope, yielding a curve that captures the underlying minimum structure of the function. To accurately capture the phase-induced variations of  $f(x)$ ,  $T$  should be less than  $\lambda$ . Moreover, the width of the sliding window should span multiple wavelengths to ensure sufficient averaging of the fluctuations in  $f(x)$ . A gradient-based method is then employed to minimize the resulting smooth and continuous function  $\bar{f}(x)$  over the interval  $0 \leq x \leq L$ . Lastly, a fine-tuning stage is performed by evaluating  $f(x)$  at  $2N + 1$  uniformly spaced points in the interval  $[x_{\text{sm}}^* - \Delta, x_{\text{sm}}^* + \Delta]$ . Here,  $x_{\text{sm}}^*$  denotes the PA position corresponding to the minimum of  $\bar{f}(x)$ ,  $\Delta = N\delta$  and should be in the order of wavelengths, and  $\delta \ll \lambda$  is the sample spacing. The minimum sample is selected, which, as  $N \rightarrow \infty$ , converges to the global minimum.

### B. Optimization of the DL scenario

In this subsection, an average BER minimization-based joint optimization method is proposed to jointly optimize the PA position  $x$ , and the power allocation coefficient  $\alpha$ . Unlike in the UL, the optimization of the DL scenario does not require any smoothing. The DL BER expression in (23) depends solely on the magnitude of the channel,  $|\tilde{h}_k(x)|$ , and therefore does not experience the rapid phase fluctuations observed in the UL case. However, in the DL scenario, both the PA location,  $x$ , and the power control coefficient,  $\alpha$ , shall be jointly optimized to minimize the average BER of the users. Unlike the UL scenario, the PA position alone is not enough to enable NOMA - if the signals intended for both UEs are transmitted with the same power, it will be impossible for each user to apply SIC and successfully decode the symbols. Therefore, the optimization problem can be formulated as

$$\min_{x, \alpha} 10 \log_{10} (\text{BER}_1^{\text{DL}}(x, \alpha) + \text{BER}_2^{\text{DL}}(x, \alpha)), \quad (26a)$$

$$\text{s.t. } 0 \leq x \leq L, \quad 0 \leq \alpha \leq 1. \quad (26b)$$

The cost function in (26a) is smooth and continuous in  $x$  and  $\alpha$  (as seen in Fig. 6 of Sec. V-B). Thus, (26) can be solved using a gradient-based method, as the cost function and constraints are continuous and have continuous first derivatives.<sup>1</sup>

<sup>1</sup>Note that the optimization procedure should be repeated with multiple random initializations to ensure convergence to the global minimum. This lies significantly below any local minimum, making it easily identifiable.

## V. NUMERICAL RESULTS

This section verifies the analytical results and explores the system behavior. We consider a PA of length  $L = 20$  m at a height of  $d = 3$  m above a  $D_1 \times D_2 = 20 \times 4$  m<sup>2</sup> environment. The attenuation factor along the dielectric is  $\kappa = 0.1$  dB/m and the effective refractive index of the dielectric is  $\eta_{\text{eff}} = 1.4$  [3]. We assume that UE 1 is located at  $(x, y) = (3, -1)$  and UE 2 is located at  $(x, y) = (18, 3)$ . In the DL scenario, the BS employs QPSK modulation to the signal intended for UE 1 and 16-QAM to the signal intended for UE 2. In the UL case, it is assumed that both UEs are transmitting at the same transmit power, that is,  $P_1 = P_2$ . The carrier frequency is set to  $f_c = 28$  GHz, and the noise variance is  $\sigma^2 = -90$  dBm. For simulated results,  $10^6$  symbols are generated.

### A. UL PA-Based NOMA

Figure 3 plots the BER of each UE and the average BER against the transmit power for an UL PA-assisted NOMA system. Results are shown for an optimally placed PA, a PA placed halfway between the UEs at  $x = 10.5$ , and a PA placed next to UE 1 at  $x = 3$ . The sliding window applied for smoothing spans  $20\lambda$ , i.e., 20 samples, and  $T = 0.01$  m.

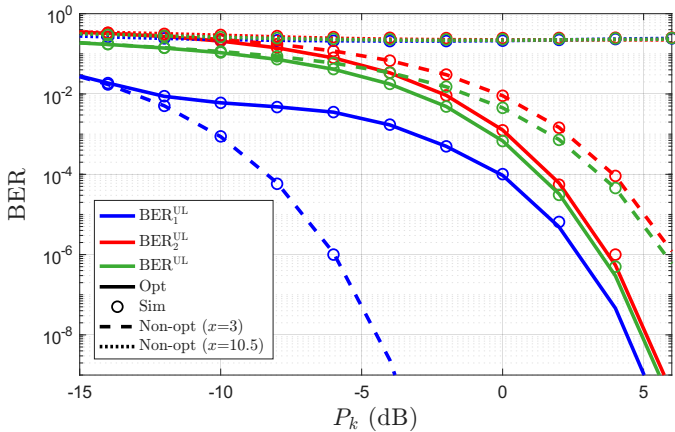


Fig. 3. BERs of each UE and the average BER in the two user UL PA-assisted NOMA system for both optimized and non-optimized PA placement.

It can be seen that there is excellent agreement between the analytical and simulated results for all scenarios considered. When the PA is located at  $x = 10.5$ , the BERs exhibit a pronounced error floor. This is a consequence of the insufficient power difference between the UEs, which prevents the effective operation of NOMA. In contrast, placing the PA at a location other than the midpoint between the two UEs removes the error floor. Given the strong distance dependence of the channel coefficient in (3), the PA can be strategically positioned to induce different path lengths between itself and the UEs, providing the power difference required for successful NOMA. These results demonstrate that a PA can be leveraged to enable NOMA and thus improve the utilization of limited spectrum.

To optimize the sum rate of a PA-based NOMA system, the best performance can often be obtained by maximizing the performance of the strongest UE [4], [8], which tends to involve placing the PA near the strong UE. However, as the

focus in this work is the average BER, it is necessary for both UEs to achieve reliable error performance. Placing the PA at  $x = 3$ , the closest position to UE 1, results in excellent BER performance for UE 1. However, the average BER is worse than the optimized case because of the degraded performance of UE 2. This shows that the optimization approach inherently ensures fairness.

Figure 4 plots the average UL BER as a function of PA position for a range of UE transmit powers, as well as the smoothed function used for the UL optimization.

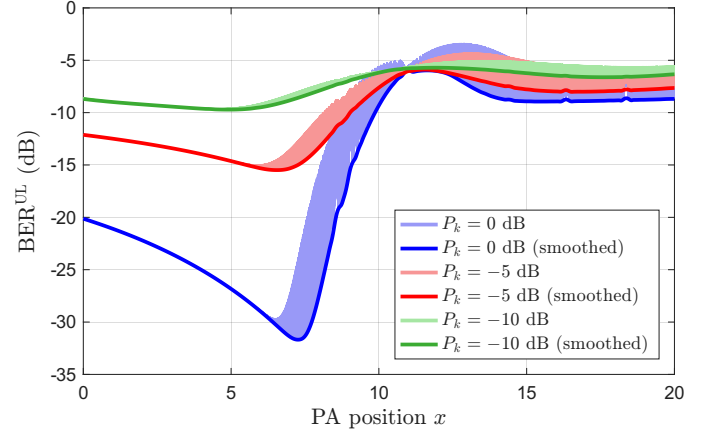


Fig. 4. Average UL BER in dB as a function of PA position.

The BER function rapidly fluctuates with antenna position for all transmit power levels. The high carrier frequency means that even a position shift in the order of millimeters corresponds to a significant fraction of the wavelength, resulting in a large phase change. For example, in some regions of the dielectric in the  $P_k = 0$  dB scenario, a PA position change of 1 mm corresponds to an average BER change of around 10 dB. These oscillations demonstrate the necessity of smoothing the objective function before optimization as outlined in Sec. IV-A.

Additionally, at lower transmit power levels, the optimal PA position shifts closer to UE 1. This is because the required power disparity between the UEs arises solely from their relative distances to the PA. At lower power, a positional change yields a smaller absolute change in received power, necessitating a larger distance difference to achieve sufficient disparity. Conversely, at higher transmit power, lower average BERs are attainable, but this requires both UEs to maintain good error performance. In all cases, the highest average BER occurs when the PA is close to equidistant from both UEs.

### B. DL PA-based NOMA

Figure 5 shows the BER of the received signal at each UE for a range of transmit powers for a DL PA-based NOMA system. Results are shown for a system jointly optimized using the method detailed in Sec. IV-B, a non-optimized system where  $x = 10$  and  $\alpha = 0.9$ , and a system where the PA position is optimized but  $\alpha = 0.5$ , leading to the signals intended for each UE being transmitted with equal power.

Again, it is evident that there is excellent agreement between simulated and analytical results. Similar to the UL case, non-optimized parameters can result in the BER of one UE being

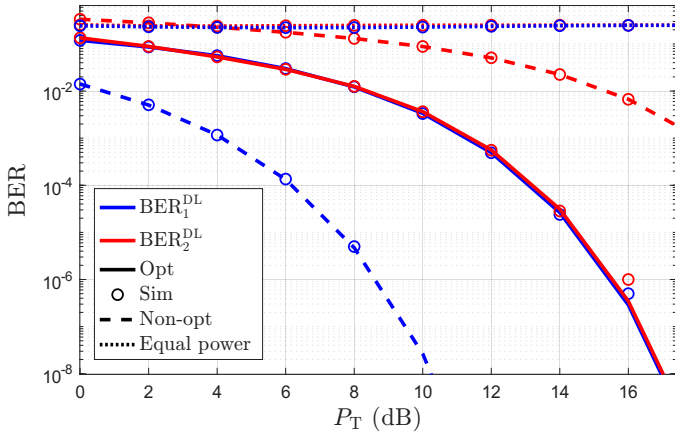


Fig. 5. BERs of each UE in a two-user DL PA-based NOMA system for both optimized and non-optimized PA placement and power control coefficients.

significantly stronger than the other. This has a negative effect on the average BER, which is dominated by the larger BER. Optimization leads to equivalent BERs for all UEs. This same result would be achieved by minimizing the maximum individual BER. However, jointly optimizing the parameters for the average BER results in a simpler optimization problem, as there is only one function being optimized rather than multiple being solved iteratively. The BER of both UEs converging to the same value after optimization is possible due to the fact that the power allocation coefficient and PA position are jointly optimized. In the UL scenario, the results in Fig. 3 show a gap between the optimized BER of UEs 1 and 2. In that scenario, both UEs transmit with equal power. Therefore, the PA position must create a sufficient power difference in the received signals from each UE to enable NOMA. This results in one UE experiencing a stronger received signal and consequently achieving a lower BER. As discussed in Sec. IV-B, in the DL case, it is not possible for PD-NOMA to function when the signals corresponding to each UE are transmitted with the same power due to interfering QAM constellations, making successful decoding at the receiver impossible. This is shown in Fig. 5, where the BERs in the equal power scenario do not improve with higher transmit powers. Figure 6 further details the impact of the relationship between the power control coefficient  $\alpha$  and the PA position on the BER; when the power is shared equally, the average BER is always high.

Figure 6 also shows that the average DL BER function is smooth. This is in contrast to the average UL BER functions shown in Fig. 4, which oscillate rapidly due to small changes in PA position leading to large changes in phase. The smoothness in the DL function is due to the unconditional BER of each UE only being a function of the magnitude of the channel  $h_k(x)$ . Moreover, unlike the UL case, there are no fluctuations arising from the superposition of two channels with different phases. However, this is unique to systems with a single PA - multiple PAs will result in channels from each being superimposed at the UEs, leading to constructive and destructive interference and thus fluctuations in the DL average BER function.

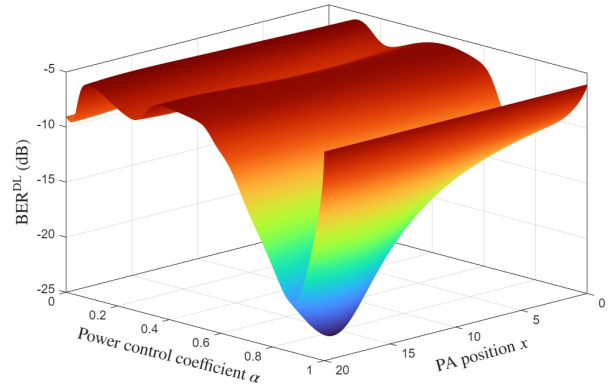


Fig. 6. Average DL BER in dB as a function of the PA position and power allocation coefficient  $\alpha$ .

## VI. CONCLUSION

This paper provided the first BER analysis of PA-based PD-NOMA systems with the aid of practical imperfect SIC decoding. We derived the exact average BER for two-user UL and DL systems. The proposed PA location optimization scheme for the UL and the joint PA–power allocation optimization scheme for the DL were shown to effectively minimize the average BERs of the two scenarios. Simulation results confirmed the accuracy of the analysis and demonstrated that the optimized PASS-NOMA system significantly outperforms the non-optimized counterpart. Both optimization methods inherently ensure fairness among UEs and eliminate error floors. The results of the optimization schemes concluded that the optimized PA location should be closer to the first user in the SIC order in the UL scenario, while the PA should be placed closer to the second user in the SIC order in the DL scenario. These findings highlight the potential of strategic PA placement to enable successful NOMA under imperfect SIC and improve the reliability and efficiency of PA-based NOMA systems.

## REFERENCES

- [1] S. Rangan, T. S. Rappaport, and E. Erkip, “Millimeter-wave cellular wireless networks: Potentials and challenges,” *Proc. IEEE*, vol. 102, no. 3, pp. 366–385, Mar. 2014.
- [2] A. Fukuda *et al.*, “Pinching antenna - using a dielectric waveguide as an antenna,” *NTT DOCOMO Technical J.*, vol. 23, no. 3, pp. 5–12, Jan. 2022.
- [3] Z. Ding, R. Schober, and H. V. Poor, “Flexible-antenna systems: A pinching-antenna perspective,” *IEEE Trans. Commun.*, vol. 73, no. 10, pp. 9236–9253, Oct. 2025.
- [4] Z. Zhou, Z. Yang, G. Chen, and Z. Ding, “Sum-rate maximization for NOMA-assisted pinching-antenna systems,” *IEEE Wireless Commun. Lett.*, vol. 14, no. 9, pp. 2728–2732, Sep. 2025.
- [5] Y. Xu, Z. Ding, and G. K. Karagiannidis, “Rate maximization for downlink pinching-antenna systems,” *IEEE Wireless Commun. Lett.*, vol. 14, no. 5, pp. 1431–1435, May 2025.
- [6] S. Lv, Y. Liu, and Z. Ding, “Beam training for pinching-antenna systems (PASS),” *IEEE Trans. Wireless Commun.*, Early Access, Sep. 2025.
- [7] H. Zhang *et al.*, “Beam focusing for near-field multiuser MIMO communications,” *IEEE Trans. Wireless Commun.*, vol. 21, no. 9, pp. 7476–7490, Sep. 2022.
- [8] K. Wang, Z. Ding, and R. Schober, “Antenna activation for NOMA assisted pinching-antenna systems,” *IEEE Wireless Commun. Lett.*, vol. 14, no. 5, pp. 1526–1530, May 2025.
- [9] M. AlaaEldin *et al.*, “RIS-enabled multi-user  $M$ -QAM uplink NOMA systems: Design, analysis and optimization,” *arXiv:2503.03972*, Mar. 2025.